Wetlands (2011) 31:989–1002
DOI 10.1007/s13157-011-0214-3

ARTICLE

Hydraulic Resistance versus Flow Depth in Everglades Hardwood Halos

David A. Chin

Received: 21 January 2011 / Accepted: 3 August 2011 / Published online: 1 September 2011

Abstract The variation of the Manning roughness with flow depth in two hardwood-dominated vegetation halos that surround water-delivery structures in Everglades National Park was investigated. The results show that the hydraulic resistance of the halos decreases approximately linearly with increasing flow depth. For flow depths less than 15–20 cm, the hydraulic resistance is similarly high in both the halo and the downstream marsh vegetation, however, as the flow depth increases the hydraulic resistance in the halo decreases to below that in the downstream marsh. As a consequence, for increased stages at the delivery structure, the halo vegetation will become less restrictive relative to the marsh vegetation in controlling water deliveries.

Keywords Hardwood · Manning · Marsh · Model · Wetlands

Introduction

Hydraulic resistance is of central importance in understanding the behavior of wetlands since it controls the flow distribution and is an important factor in nutrient and sediment transport, the evolution of vegetative communities, and the morphology of the landscape. In managed wetlands such as the Florida Everglades, water is delivered at some locations by structures that terminate in stilling pools. Exotic vegetation typically surrounds these pools due the high sediment and nutrient loads in the delivered water, and the surrounding areas of exotic vegetation are sometimes referred to as "halos". In cases where these halos are dominated by hardwood species, they are called hardwood halos. The vegetation architecture in a hardwood halo is significantly different than in marsh vegetation, and it is an open question as to whether this difference in vegetation architecture is sufficient to cause significant differences in hydraulic resistance between the hardwood halo and the downstream marsh. Since halos of exotic vegetation can generally be expected downstream of water-delivery pools, accurate characterization of the hydraulic resistance of these areas can have a significant influence on the management of water deliveries to wetlands.

The primary sources of hydraulic resistance in marsh wetlands are the vegetation and the ground surface, with the submerged and emergent vegetation usually being the dominant sources of resistance. Parameters that have been used to characterize hydraulic resistance in wetlands are the stem/leaf drag coefficient (Nepf 1999), the bulk drag coefficient (Lee et al. 2004), and the Manning roughness (Variano et al. 2009). Parameterizing the hydraulic resistance in terms of a drag coefficient is more robust than using a Manning roughness, since using a constant Manning roughness with the associated Manning equation implicitly assumes that the resistance is due entirely to protruding roughness elements on the bed of the wetland and implies that

Electronic supplementary material The online version of this article (doi:10.1007/s13157-011-0214-3) contains supplementary material, which is available to authorized users.

D. A. Chin (✉)
Department of Civil, Architectural, and Environmental Engineering, University of Miami, 1251 Memorial Drive, Coral Gables, FL 33146, USA
e-mail: dchin@miami.edu

the flow is fully turbulent (Chin 2006); neither assumption is typically valid (Lee et al. 2004). An approach to circumvent this conceptual dilemma was suggested by Kadlec (1990), who used a flow model in which the flow velocity was related empirically to the flow depth and energy gradient, thereby avoiding the use of Manning's n altogether. However, as a practical reality, most large-scale hydrodynamic models of wetland flow parameterize the hydraulic resistance in terms of the Manning roughness and utilize the Manning equation to characterize the drag forces exerted by both the vegetation and the bed. Adjustment of the Manning roughness is the usual means of calibrating wetland hydrodynamic models.

Laboratory-scale experiments of flow through emergent marsh vegetation have been reported by Nepf (1999) and Lee et al. (2004). Expressing the results of these experiments in terms of a Manning roughness, Nepf (1999) indicated that the Manning roughness is proportional to the flow depth raised to the two-thirds power, and Lee et al. (2004) indicated that the Manning roughness is both proportional to the flow depth raised to the two-thirds power and inversely proportional to a depth-based Reynolds number. A summary of several other experimental results reported by Tsihrintzis (2001) and Tsihrintzis and Madiedo (2000) support the functional form of the Manning roughness reported by Lee et al. (2004). There have been a limited number of field-scale studies on the relationship between the Manning roughness and flow depth, which can be attributed to a variety of factors, including the difficulty in measuring flow velocities at small depths, the difficulty in measuring spatial variations in flow velocities, the difficulty in accurately measuring stage gradients over relatively small distances, and the difficulty in accurately measuring topographic variations over small distances. For the most part, field investigations have corroborated the laboratory results in that they indicate that the Manning roughness is proportional to the depth raised to the two-thirds power and inversely proportional to the Reynolds number. Detailed flow measurements in the Everglades reported by Harvey et al. (2009) and further analyzed by Larsen et al. (2009) indicate that the appropriate Reynolds number is based on the stem-diameter, while field measurements reported by Lee et al. (2004) indicate that the appropriate Reynolds number is depth based. Collectively, these results agree that in wetlands with uniform emergent vegetation and transitional or turbulent flows within the canopy, the Manning roughness can be taken as proportional to the flow depth raised to the two-thirds power. Variano et al. (2009) and He et al. (2010) used field measurements of flow and hydraulic gradient to estimate the Manning roughness in the Everglades, however the relationship to flow depth was not investigated.

Previous laboratory and field investigations of wetland flow through emergent vegetation are mostly applicable to cases where the architecture of the submerged portion of the emergent vegetation does not change significantly with depth of flow and variations in the bed topography, and variations in available flow paths do not significantly influence the flow. These conditions are typical of marsh flows; however, in hardwood-dominated wetland forests the preferential flow paths can be significantly influenced by vegetation architecture, bed topography, and depth of flow, particularly at low flow depths. As a consequence, an alternative model similar to that proposed by Luhar et al. (2008) in which a blockage factor decreases with increasing flow depth might be more appropriate, in which case the effective Manning roughness could decrease with increasing flow depth.

The objective of this investigation was to use field-scale measurements to determine the variation of the Manning roughness, n, with flow depth, h, in the hardwood-dominated halos that surround some of the water delivery structures in Everglades National Park. The results of this investigation are novel in that there have been no previous investigations of n versus h in hardwood dominated wetlands in south Florida.

Site Description

This study was conducted in Everglades National Park (ENP), located in southern Florida where the average annual air temperature is 24°C and the average annual precipitation is 1320 mm (Duever et al. 1994). The northern boundary of ENP includes a 17.2-km section of the US41 roadway commonly known as Tamiami Trail where water is delivered to ENP by several three-barrel culvert structures as shown in Fig. 1. The source of water at each delivery structure is the L29 canal on the north side of Tamiami Trail, where stages within the L29 canal are controlled by gated-spillways (S333 and S334) at the western and eastern ends of the canal. The water-delivery structures of interest in this study are the culverts designated as C43 and C51, and a typical tailwater view of the C51 structure is shown in Fig. 1. The stages in the L29 canal are regulated so as not to exceed a maximum stage of 1.83 m relative to the North American Vertical Datum of 1988 (NAVD 88), and the culvert structures have tailwater pools with approximate dimensions of 22 m × 14 m at C43 and 15 m × 14 m at C51.

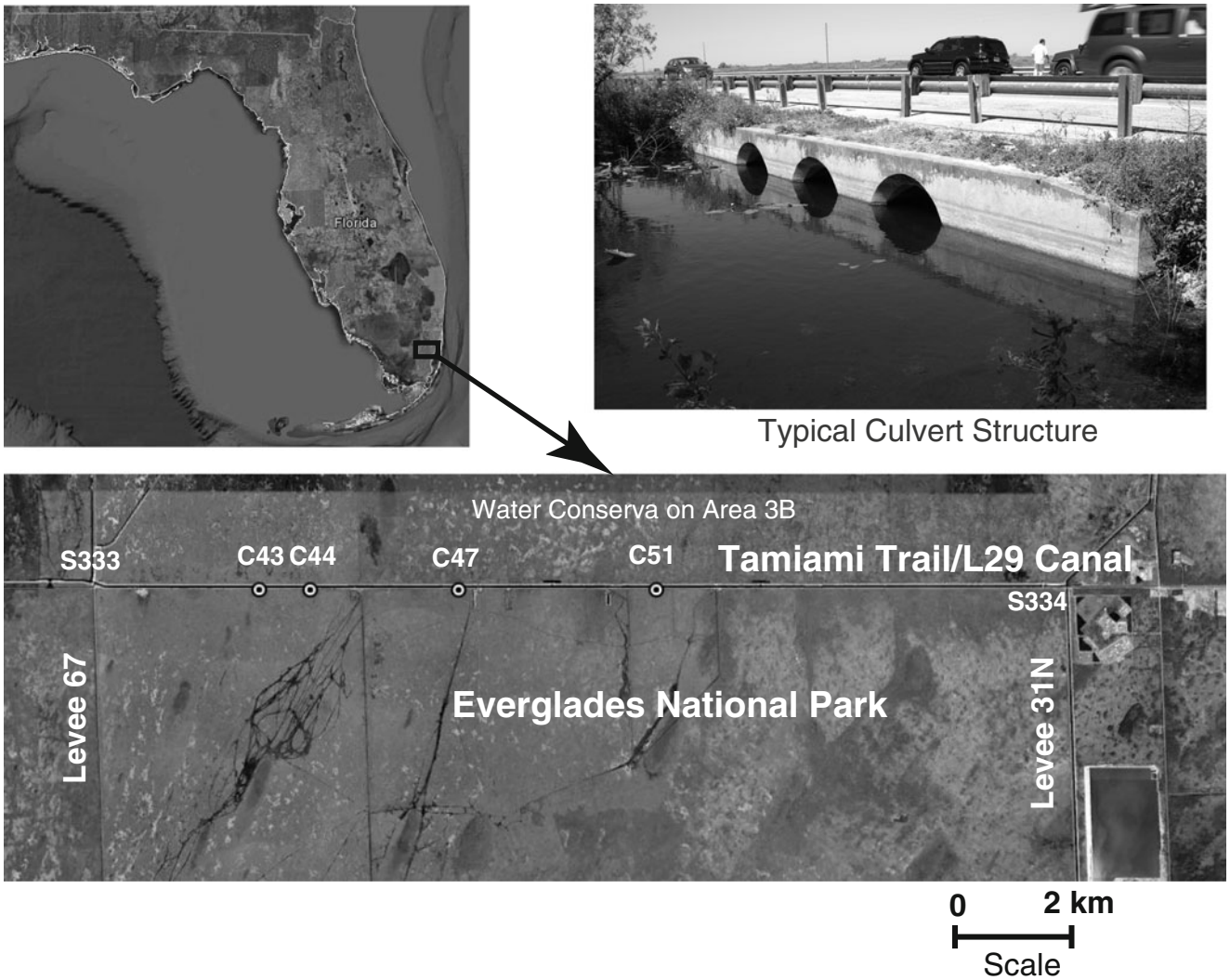

Fig. 1 Locations of the C43 and C51 study sites as well as a typical culvert structure at each site. All sites are located on the northern boundary of Everglades National Park in south Florida. Aerial photography from Google Earth, May 2009.

Aerial views of the C43 and C51 study sites are shown in Fig. 2a and c, respectively, where the tailwater pool downstream of the culvert delivery structure is located at point A. The plant communities downstream of the tailwater pools were identified by field reconnaissance. At both study sites, two distinct plant communities were apparent: a wetland hardwood-dominated community immediately downstream of the tailwater pool, and a sawgrass-dominated community downstream of the wetland hardwood community. The hardwood-dominated community is referred to as the "halo", and primarily consists of pond apple (*Annona glabra*), Brazilian pepper (*Schinus terebinthifolius*), which is an invasive exotic, and Carolina willow (*Salix caroliniana*), with an understory of herbaceous native plants dominated by leather fern (*Arostichum danaeifolium*). The hardwood community also contained some fallen trees and tree branches. The sawgrass community is dominated by sawgrass (*Cladium jamaicense*), and the transition zone included some cattail (*Typha domingensis*). The location of the transition from the hardwood community to the sawgrass community (i.e., the halo boundary) was estimated from color aerial photographs, and the estimated halo boundaries are shown in Fig. 2a and c for the C43 and C51 sites, respectively. This delineation between the hardwood dominated halo and the downstream marsh area is particularly relevant to the flow model used in the study, since the hardwood community (halo) could have different hydraulic roughness characteristics than the sawgrass-dominated plant community. Water depths typically increased with downstream distance

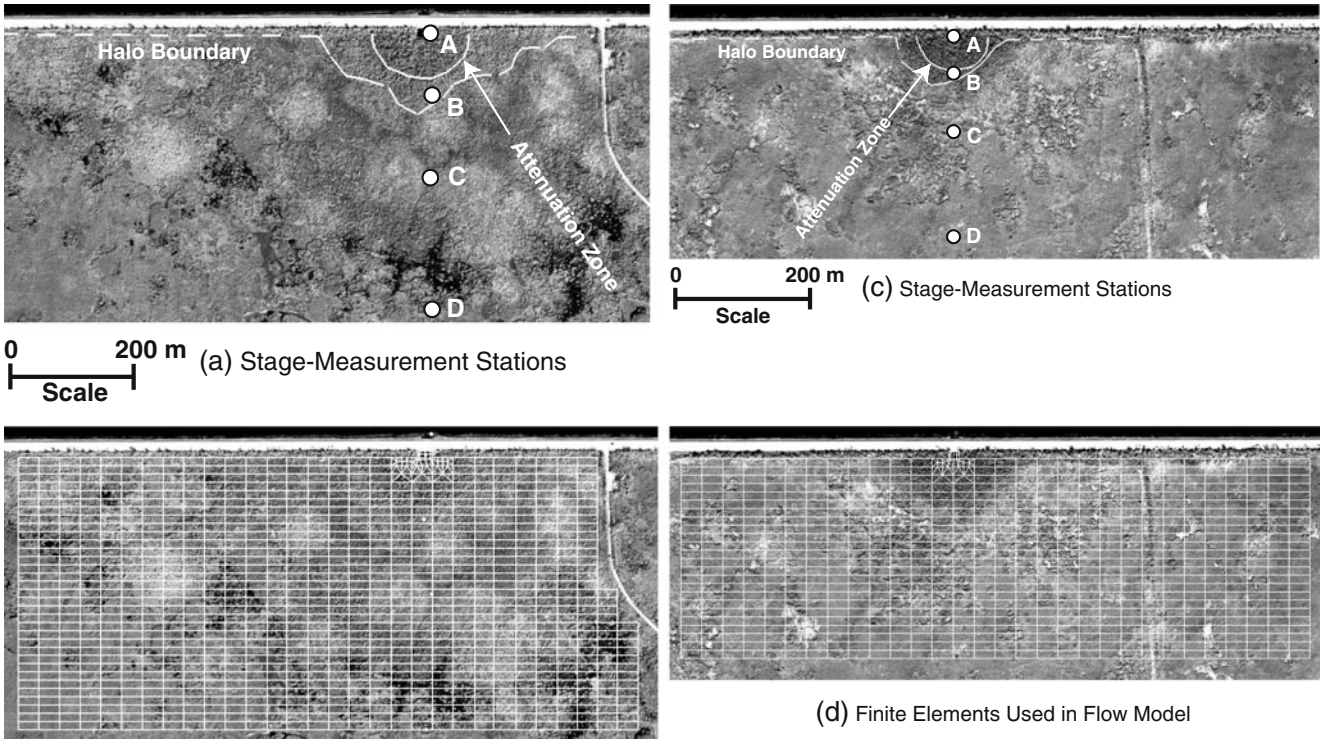

Fig. 2 **a** Aerial view of the C43 study site and locations where stages were measured at 15-min intervals, the measurement locations are denoted by A, B, C, and D. The region where the stage is 90% attenuated (as calculated by the numerical flow model) is denoted as the attenuation zone, and the boundary of the hardwood vegetation halo surrounding the tailwater pool (as delineated by visual inspection of aerial color photographs) is also identified. Flows enter the study area via inflows to the tailwater pool at A. **b** Finite-element grid used in the flow model, which was derived from the RMA-2 code (USACE 2008). **c** and **d** are same as (**a**) and (**b**) but for C51 site. Aerial photography from USGS Map Server, May 2009

from the tailwater pool, with maximum depths usually between 50 and 55 cm and occasionally as high as 65 cm. The minimum water depth was generally 0 cm near the upstream boundary of the study area adjacent to the US41 roadway. The study areas did not contain any discernible ridge and slough characteristics, with the vegetation being typical of Everglades ridges (Larsen et al. 2009). The estimated area of the halo at the C43 site is 2.2 ha, with the surrounding marsh area in the study domain covering approximately 33 ha. At the C51 site, the halo covers approximately 0.7 ha and the surrounding marsh covers about 26 ha. Measurements of plant density in the hardwood halo and surrounding marsh areas were not made; however, it was apparent from visual observation that plant densities were nonuniform in both areas. In the halo areas the vegetation was relatively sparse and became denser with increasing distance from the tailwater pool. The marsh areas consisted of dense sawgrass immediately downstream of the halos, with more open areas and less dense marsh towards the downstream ends of the study areas.

Methods

Field data collected during this study included measurements of flow through the C43 and C51 culvert structures into ENP, and the stage distribution and ground topography downstream of these structures. The study was conducted between June 2009 and September 2010. The measured data were used to calibrate a steady-state hydrodynamic (backwater) model to identify the Manning roughness, n, that provides the best match with observations, and the relationship between n and flow depth was derived from these results.

Flow Measurements

The flow in the center barrel of each culvert structure was measured using an Argonaut-SW™ acoustic Doppler current profiler (ADCP) (SonTek/YSI Inc., San Diego, CA, firmware version 11.8) attached to the bottom of the center barrel and approximately 3 m upstream from the outlet. The Argonaut-SW™ is a pulsed Doppler current profiling system that uses a monostatic transceiver configuration, where the acoustic transducers both transmit and receive the acoustic signals. The Argonaut-SW™ has three acoustic beams. One of these beams is directed vertically and the other two point upstream and downstream at a 45-degree angle to the vertical. The mean velocity in the culvert barrel was computed from the vertically integrated velocity profile using an algorithm based on the 1/6th-power velocity distribution model (Chen 1991). Each ADCP was programmed to sample the vertical velocity profile for 2 min and to compute the corresponding vertically averaged velocity at 15-min intervals. The instrument had a blanking distance of 7 cm and bin (cell) sizes of 20 cm; typical depths of flow above the ADCP were 135 cm at C43 and 105 cm at C51. During the 2-min averaging interval, the ADCP collected 120 velocity profiles and depth measurements that were internally averaged prior to logging the data. The standard error in the velocity measurements given by the manufacturer is 0.5 cm/s. Flowrate errors of 10–20% were estimated for typical flows at the C43 site, and 5–10% for typical flows at the C51 site.

Velocities at the culvert outlets were manually measured using a FlowTracker™ hand-held acoustic Doppler velocity (ADV) meter (SonTek/YSI Inc., San Diego, CA, firmware version 3.3). At each of the three barrel outlets at each culvert structure, FlowTracker™ measurements were taken at 20%, 60%, and 80% of the flow depth, and the average velocity in each culvert barrel was obtained from these measurements using the three-point averaging method. The three-point averaging method is appropriate in this case since there is no assurance that the velocity distribution is logarithmic (Sauer 2002). The vertically averaged velocity, V_{FT}, in each culvert barrel estimated by the three-point method is given by

$$V_{FT} = \frac{1}{4}(v_{0.2} + 2v_{0.6} + v_{0.8}) \quad (1)$$

where $v_{0.2}$, $v_{0.6}$, and $v_{0.8}$ are the measured velocities at 20%, 60%, and 80% of the depth, respectively. The FlowTracker™ measurements were primarily used to establish the partitioning of flow between culvert barrels, and these partitioning results were used in combination with the ADCP measurements in the center barrel to provide a (quasi-)continuous record of total flow through the culvert structure. The distribution of flows between culvert barrels derived from the FlowTracker™ measurements at the C43 and C51 structures are shown in Fig. 3. These results give the median and 25–75 percentile ranges of the fractions of total flow in each culvert barrel, where outliers were defined as measurements that were more than 150% of the 25–75 percentile range from either the 75-percentile or 25-percentile value. Outliers were typically associated with very low flows where it was difficult to accurately establish the flow distribution between barrels. The distribution of measured flow fractions shown in Fig. 3 generally supports the assumption that one-third of the flow goes through each culvert barrel such that the flow is distributed equally between the barrels. Based on these results, the total flow through each culvert structure was taken as the flow measured by the ADCP in the middle barrel multiplied by three. The same flow-measurement protocol was applied at the C43 and C51 sites, with the only difference being that the diameter of the culvert barrels was 152-cm at C43 and 122-cm at C51.

Flows measured by the ADCP and FlowTracker™ in the center barrel were similar although not directly comparable since the ADCP was mounted inside the culvert barrel approximately 3 m from the exit, while the FlowTracker™ measurements were taken at the culvert exit and were more influenced by exit conditions.

Topography Measurements

At both study sites, the topography downstream of the tailwater pool was measured using global positioning system real-time kinematic (GPS RTK) instrumentation (Trimble, Inc., Sunnyvale, CA, R8 GNSS GPS receiver, TSC2 Data Controller, REA 96W radio transmitter). The topographic measurements were taken at intervals of approximately 6.1 m in the north-south direction (outward from the delivery structure) and intervals of 30.5 m in the east-west direction. The rationale for a denser spacing in the north-south direction was that more rapid variations in ground elevation occurred in the north-south direction compared to the east-west direction. In the immediate vicinity of the tailwater pool, there were much denser and irregular topographic measurements. The accuracy of elevation measurements determined by the GPS RTK system was estimated by comparing repeat measurements of several fixed points with the study area, and these results showed that a standard error of approximately

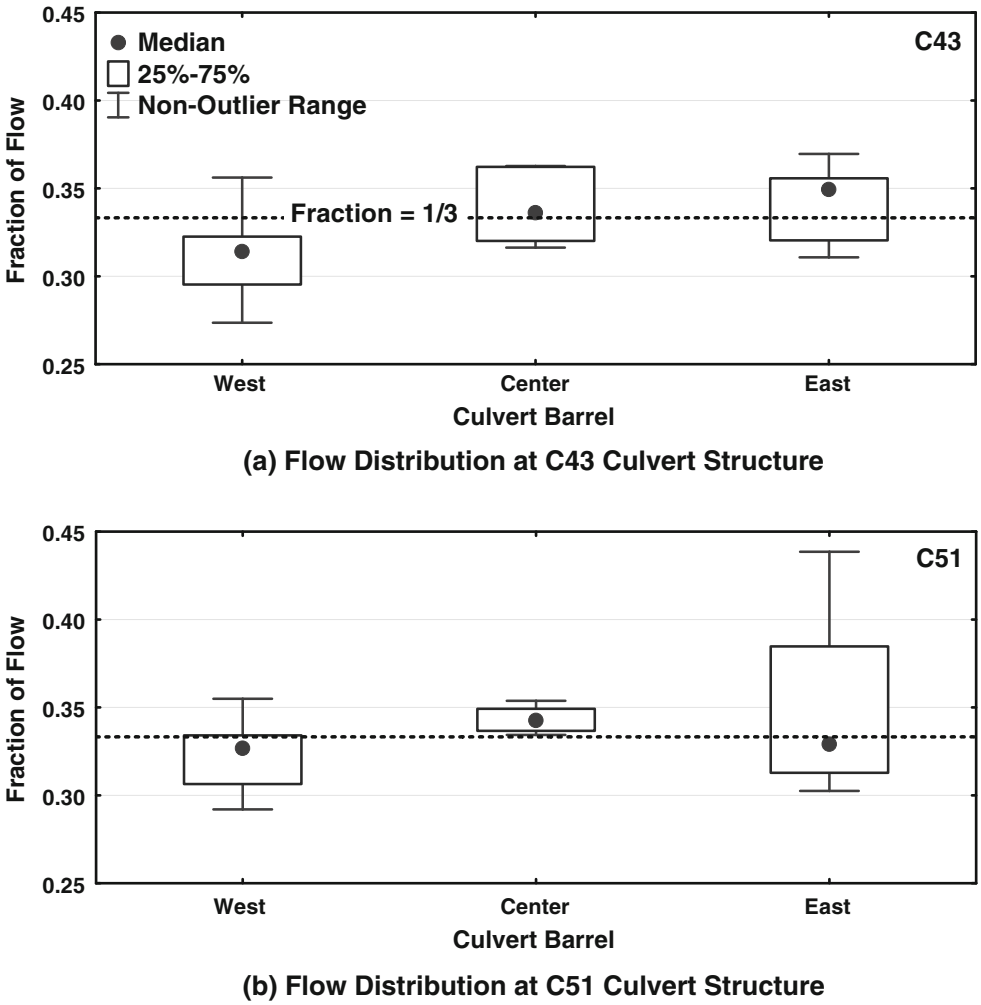

Fig. 3 Fractional distribution of flows between culvert barrels at the C43 culvert structure as derived from the FlowTracker™ measurements is given in (**a**), and the flow distribution for the C51 culvert structure is given in (**b**)

1.5 cm could be associated with each measurement. At each study site, the measured elevations were absolute and derived from U.S. Army Corps of Engineers benchmark monuments at the culvert locations, where benchmark FCE 5106 was used at C43 and benchmark FCE 5096 was used at C51. All elevations were measured relative to the North American Vertical Datum of 1988 (NAVD 88). The locations of topographic measurements coincided with the node locations of the finite elements shown in Fig. 2b and d. Topographic maps of the study sites derived from the measured elevations are shown in S1. At both sites, higher bed elevations are found surrounding the inflow locations, and these higher elevations form ridges that are mostly surrounded by lower bed elevations.

Stage Measurements

Water-surface elevations (stages) were measured using HOBO™ pressure transducers (Onset Computer Corporation, Bourne, MA, U-20 Water Level Logger). At each study site, continuous stage measurements were taken at locations A, B, C, and D shown in Fig. 2a and c for the C43 and C51 sites, respectively. The distance AD is 402 m at the C43 site and AD is 292 m at the C51 site, and at both sites AB is 25% of AD, and AC is 50% of AD. At both study sites station A was located in the tailwater pool at least 5 m from the culvert exit, and so any turbulence caused by the culvert discharge was dissipated before reaching station A. At all stage-measurement locations, the transducers were suspended within stilling wells that consisted of 50-mm diameter PVC pipes with meshed screens at the bottom and locked caps at the top. All stilling wells used to house the pressure transducers were attached to steel poles for stability. The transducers used to measure stages each contain a Motorola MPX-series pressure transducer coupled with a miniature data logger. According to the manufacturer, the accuracy of water-level measurements is on the order of 0.005 m. The transducers were programmed to record stages every

15 min and were synchronized with measurements of flow through the culvert structures.

Water-surface elevations recorded by the transducers were measured relative to the elevation of the transducer in the stilling well, and adjustment of these measurements to NAVD 88 stage elevations required manual stage measurements at the beginning and end of each deployment, as well as adjustment relative to synoptic atmospheric pressure measurements. Manual measurements of water stages at the beginning and end of each deployment were performed by measuring the depth to water (DTW) from the top of the stilling well, and then the actual water-surface elevation was computed by subtracting the DTW from the known elevation of the top of the stilling well. Reference elevations at the top of the stilling wells were measured using the same GPS RTK instrumentation used to measure the topography. Depth-to-water measurements were generally taken in triplicate using marked tape measures with increments of 0.0008 m. Tape marking was done using washable markers to identify the water line. Synoptic measurements of atmospheric pressure were collected using a transducer mounted above the water surface in one of the stilling wells (51A). It was assumed that this measured atmospheric pressure was representative of the atmospheric pressure at all stilling-well locations at both the C43 and C51 sites.

Flow Model

Steady-state flows at the study sites were described by the depth-integrated continuity and momentum equations given, respectively, by

$$h\left(\frac{\partial u}{\partial x}+\frac{\partial v}{\partial y}\right)+u\frac{\partial h}{\partial x}+v\frac{\partial h}{\partial y}=0 \tag{2}$$

$$hu\frac{\partial u}{\partial x}+hv\frac{\partial u}{\partial y}-\frac{h}{\rho}\left[E_{xx}\frac{\partial^2 u}{\partial x^2}+E_{xy}\frac{\partial^2 u}{\partial y^2}\right]+gh\left[\frac{\partial a}{\partial x}+\frac{\partial h}{\partial x}\right]+\frac{gun^2}{\left(h^{1/6}\right)^2}(u^2+v^2)^{1/2}=0 \tag{3}$$

$$hu\frac{\partial v}{\partial x}+hv\frac{\partial v}{\partial y}-\frac{h}{\rho}\left[E_{yx}\frac{\partial^2 v}{\partial x^2}+E_{yy}\frac{\partial^2 v}{\partial y^2}\right]+gh\left[\frac{\partial a}{\partial y}+\frac{\partial h}{\partial y}\right]+\frac{gvn^2}{\left(h^{1/6}\right)^2}(u^2+v^2)^{1/2}=0 \tag{4}$$

where h is the water depth, u and v are the components of the flow velocity in the x and y Cartesian directions, respectively, t is time, ρ is the density of water, E_{xx}, E_{yy}, E_{xy}, and E_{yx} are the components of the eddy viscosity tensor, g is gravity, a is the bottom elevation, and n is the Manning roughness coefficient.

The RMA-2 computer code (U.S. Army Corps of Engineers, USACE 2008) was used to provide a numerical solution to these equations. The finite-element grid network used at the C43 site is shown in Fig. 2b, where the nodes of the finite elements were chosen to coincide with topographic measurement locations, which minimizes the error introduced by interpolating the ground topography from the discrete topographic measurements. The 12 m × 30 m finite elements downstream of the tailwater pool and the denser elements in the immediate vicinity of the pool are apparent from Fig. 2b for the C43 site and Fig. 2d for the C51 site. Eddy viscosities must be specified to quantify subgrid velocity fluctuations and, in accordance with the recommendation of USACE (2008), eddy viscosities in Eqs. 2 to 4 were automatically calculated to maintain an element Peclet number of 20, where the Peclet number, Pe, is defined as

$$\mathrm{Pe}=\frac{\rho V L}{E} \tag{5}$$

where E is the component of the eddy viscosity tensor in the flow direction (the transverse component of the eddy viscosity relative to the flow direction is taken as zero), V is the flow velocity in the finite element, and L is the length of the finite element in the flow direction. The approximation that Pe = 20 is based on the assumption that the eddy viscosity is of the same order of magnitude as the mass diffusion coefficient, and the assumed value of Pe = 20 is consistent with field measurements in the Everglades by Ho et al. (2009) who reported $3 \le \mathrm{Pe} \le 40$. Variano et al. (2009) reported $6 \le \mathrm{Pe} \le 41$, and Huang et al. (2008) reported $15 \le \mathrm{Pe} \le 44$.

The study areas at the C43 and C51 sites are the areas covered by the finite-element grids shown in Fig. 2b and d, respectively. The flow into each study area originates from the tailwater pool at the northern end and exits normal to the open boundary at the southern end. Previous studies in this area have indicated that groundwater seepage into the study areas is negligible (Wang et al. 2007), so groundwater seepage was neglected. At the C43 site shown in Fig. 2b, elevated roadways on the northern and eastern boundaries restrict the flow to be parallel to these boundaries, and the flow was also restricted to be parallel to the western boundary of the study area, which corresponds to a line of flow symmetry between the C43 culvert structure and an almost identical adjacent culvert structure. In the numerical model, upstream boundary conditions were a specified constant inflow into the tailwater pool and no-flow normal to other portions of the upstream boundary (which are adjacent to the roadway), no-flow normal

to the eastern and western boundaries, and the downstream boundary condition was a specified constant stage. At the C51 site shown in Fig. 2d, the elevated roadway on the northern boundary (Tamiami Trail) restricted flow to be parallel to this boundary. Previous studies and field measurements in this area indicate a predominantly southerly flow direction (Wang et al. 2007), which is supported by obvious north-south flow channels in the C51 topographic map shown in S1(b). Based on these considerations, flow was assumed to be in a north-south direction at the eastern and western boundaries, and normal to the southern boundary of the model. It is noted that by taking the western and eastern boundaries to be 400 m and 500 m, respectively, from the 15-m wide tailwater pool, the effects of assuming north-south flow at lateral boundaries on flow conditions in the vicinity of the tailwater pool is likely to be minimal, since these boundaries are both at least 26 pool-widths from the tailwater pool. In summary, upstream boundary conditions were a specified constant inflow into the tailwater pool and no-flow normal to other portions of the upstream boundary, flows were parallel to the eastern and western boundaries, and the downstream boundary condition was a specified constant stage.

Model Application

Field measurements were used to estimate the steady-state relationship between the flow rate through the wetland and the stages at the upstream and downstream ends of the study areas. For any observed flow condition, the value of n in Eqs. 2 to 4 that provides the best match with the field data is the appropriate n value for that flow condition. Different flow conditions correspond to different flow depths and Manning's n values, and so the relationship of n versus flow depth is derived from the different flow conditions.

The measured relationship between flow and stage at the C43 site is shown in Fig. 4a–c, where each figure corresponds to a different downstream stage, z_D, where z_D is equal to the stage measured at station D as shown in Fig. 2a. All stages are relative to NAVD 88. Values of z_D were initially divided into intervals of 0.0305 m (0.1 ft), and only those stage intervals containing synoptic stage and flow measurements over the entire range of flows being analyzed (0–0.42 m^3/s) were selected for further analysis and for use in model calibration. Data that met this criterion are shown in Fig. 4a–c, and correspond to the stage intervals of $z_D = 1.738 \pm 0.015$ m (5.7±0.05 ft), $z_D = 1.768 \pm 0.015$ m

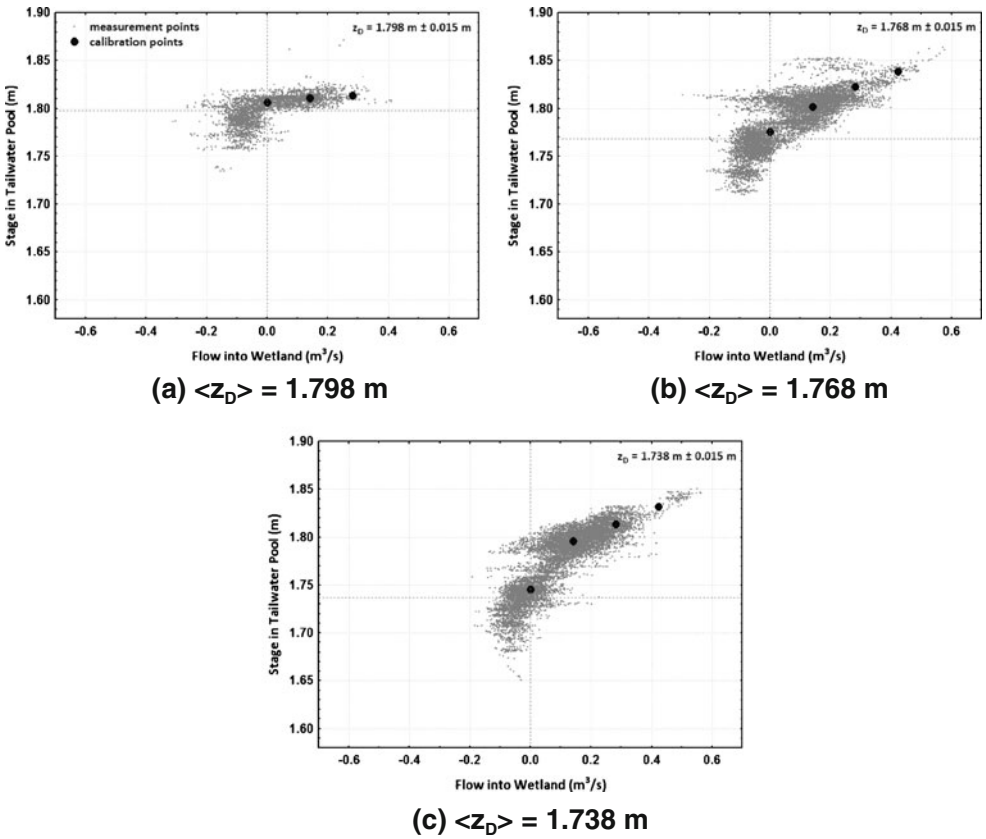

Fig. 4 Measured stages, z_A, in the tailwater pool versus measured flows into the C43 site as a function of measured stages, z_D, at the downstream end of the study area.
a $z_D = 1.798 \pm 0.015$ m.
b $z_D = 1.768 \pm 0.015$ m.
c $z_D = 1.737 \pm 0.015$ m. The large dots show the points that were used in calibrating the steady-state flow model

(5.8±0.05 ft), and $z_D = 1.798 \pm 0.015$ m (5.9±0.05 ft). To illustrate the use and meaning of Fig. 4a–c, consider first Fig. 4a. In deriving Fig. 4a, the measured synoptic flow and stage data were first filtered to contain only cases where 1.783 m $< z_D <$ 1.813 m , denoted by $z_D = 1.798 \pm 0.015$ m. Considering only these filtered data, the stage in the tailwater pool, z_A, was plotted versus the inflow, Q, where z_A is equal to the stage measured at station A (at the upstream end of the study area), and the flow, Q, is equal to the measured flow through the culvert structure into the study area; all measurements are taken at 15-min intervals. The vertical dashed line in Fig. 4a corresponds to $Q = 0$ m^3/s, and therefore divides inflows ($Q > 0$ m^3/s) and outflows ($Q < 0$ m^3/s) at the upstream end of the study area. The horizontal dashed line in Fig. 4a corresponds to $z_A = z_D$.

Flows and stages at the C43 and C51 sites changed slowly relative to the time scale for disturbances to propagate from station A to station D (around 30 min), and so most synoptic flow and stage measurements can be taken as being at approximately steady state, although random fluctuations of stage and flow measurements associated with instrument error were ubiquitously manifested in random fluctuations about true values. A typical one-month series of measurements is shown in Fig. 5 for the C43 site, where it is apparent that stages at A and D adjust fairly rapidly to each other thereby creating an approximate steady-state relationship. A few sporadic anomalous measurements

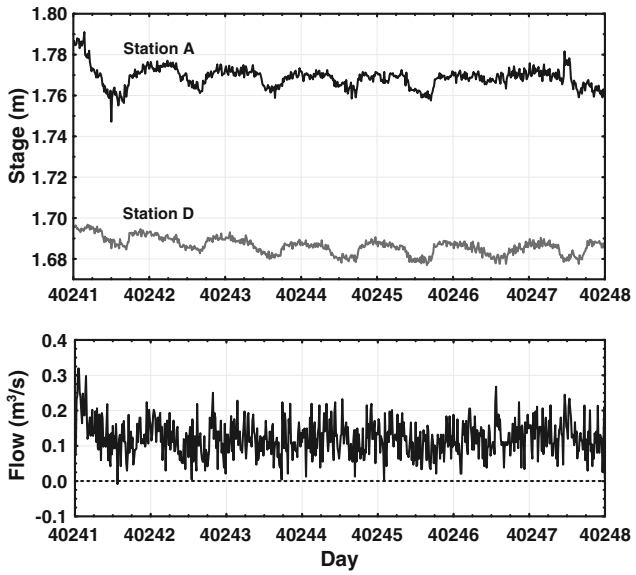

Fig. 5 Synoptic changes in stage at stations A and D compared with corresponding flows. Typical data at C43 collected every 15 min for 7 days

are also apparent in Fig. 5, such as a negative flow with a positive gradient and a sudden shift in stage at station A without a corresponding shift at station D; however, these localized occurrences are relatively infrequent and appear as outliers within the data set. Major transients in flow and stage at the C43 and C51 sites were caused primarily by the raising and lowering of stages in the upstream delivery canal associated with the operation of the S333 gated spillway; however, structure operation was relatively infrequent compared to the length of the stage and flow record. Based on these considerations, it is expected that the average measured relationship between flow and stage closely indicates the relationship that would occur under various steady-state conditions. To confirm this assumption, under steady-state conditions it is expected that on average $Q > 0$ m^3/s when $z_A > z_D$ and $Q < 0$ m^3/s when $z_A < z_D$, which is approximately confirmed on reference to Fig. 4a and indeed by all plots of stage versus flow.

Steady-state calibration points were defined as the synoptic values of Q and z_A that are likely to exist for any given value of z_D. These calibration points are shown as large dots in Fig. 4a for flows of 0, 0.14, 0.28, and 0.42 m^3/s. The calibration value of z_A for any given flow was approximated by the median value of z_A for all measured flows within ±0.07 m^3/s of the given flow. Some rounding was done in selecting the final calibration value of z_A, with the rounded values being typically within 0.003 m (0.01 ft) of the calculated medians. Negative flows were not selected for calibration since such flows were typically small and were likely to induce significantly different flow distributions in the marsh compared to positive flows. The protocol used in deriving Fig. 4a was repeated for $z_D = 1.768 \pm 0.015$ m and $z_D = 1.738 \pm 0.015$ m, and these results are shown in Fig. 4b and c, respectively. It is apparent from Fig. 4 that in some cases $Q = 0$ m^3/s does not exactly correspond to $z_A = \langle z_D \rangle$, where $\langle z_D \rangle$ is the expected value of z_D, equal to 1.798 m, 1.768 m, and 1.738 m in Fig. 4a–c, respectively. This discrepancy, Δ, was defined as

$$\Delta = |z_{A0} - \langle z_D \rangle| \tag{6}$$

where z_{A0} is the stage in the tailwater pool corresponding to $Q = 0$ m^3/s under steady-state conditions as estimated from the calibration points in Fig. 4. A plausible explanation for this discrepancy (i.e., $\Delta \neq 0$ m) is an error in surveying the reference (top-of-well) elevation at station A and/or station D, since the stage at each monitoring location was measured by assuming that the top-of-well elevation at that location is exactly

correct. Possible errors in the measured reference (top-of-well) elevations at stations A and D were estimated by performing a second survey of these reference elevations, with the difference between the first and second surveyed elevations providing a measure of the possible elevation errors in Fig. 4. It was found that the discrepancy, Δ, was generally less than the difference in surveyed elevations and so this source of error was accepted as plausible. The value of Δ in Fig. 4a–c is 0.8 cm.

The analysis protocol used to obtain the steady-state calibration points shown in Fig. 4 for the C43 site was repeated at the C51 site, and the results are shown in S4 for $z_D = 1.798 \pm 0.015$ m, $z_D = 1.768 \pm 0.015$ m, $z_D = 1.737 \pm 0.015$ m, and $z_D = 1.707 \pm 0.015$ m, respectively, where all stages are relative to NAVD 88. For the C51 site, flows were generally less than at the C43 site, and the measured data only allowed calibration points to be estimated for flows of 0, 0.14, and 0.28 m^3/s. The discrepancy, Δ, between z_{A0} and $\langle z_D \rangle$ was estimated at the C51 site as 1.2 cm, which was also attributed to surveying error since this discrepancy was less that the difference in elevation resulting from a two surveys of the reference elevations at stations A and D.

A salient feature of Fig. 4 and S4 is that they both indicate that, for any given stage difference between A and D, the flow in the wetland increases as the stage at D increases. This observation indicates that the hydraulic resistance between A and D decreases with increasing stage.

Stage measurements at intermediate stations B and C were used to validate the hydrodynamic model which was calibrated using stage measurements at stations A and D. In order to use the measurements at B and C for validation, it was necessary to remove any stage bias caused by errors in the reference elevations at B and C. To identify the bias, the stage difference between B and D, $z_B - z_D$, and the stage difference between C and D, $z_C - z_D$, were plotted as a function of the flow, Q. The bias at B was then defined as the value of $z_B - z_D$ when $Q = 0$ m^3/s, and the bias at C was defined as the value of $z_C - z_D$ when $Q = 0$ m^3/s. The biases at B and C were found to be 1.03 cm and -0.84 cm, respectively. (The data plots used to derive these biases are shown in S2.) Assuming that the stage elevations measured at D are correct, 1.03 cm was subtracted from the measured elevations at B and 0.84 cm was added to the measured elevations at C. A similar procedure was followed at the C51 site, where it was found that the bias at B is 3.13 cm and the bias at C is 0.65 cm. (The data plots used to derive these biases are shown in S3.) These biases were subtracted from the measured stage data at B and C to account for errors in the surveyed reference elevations, and the corrected elevations at these stations were used to validate the hydrodynamic model, which predicts the stages at B and C by assuming that the measured stage at D is correct.

At each of the study sites, the respective hydrodynamic models were calibrated by adjusting Manning's n such that the stages z_A and z_D for a given flow, Q, exactly matched the calibration points shown in Fig. 4 and S4. After calibration, the accuracy of the calibrated model in predicting stages within the marsh was validated by comparing the model-predicted stages at stations B and C with the measured stages at these locations, which were previously corrected to remove biases caused by errors in establishing the reference elevations. The comparative results at the C43 site for $Q = 0.28$ m^3/s (a typical observed flow) are shown in Fig. 6 for $z_D = 1.737$ m, 1.768 m, and 1.798 m, where all stages are relative to NAVD 88. It is apparent from these results that the stages predicted by the hydrodynamic model (solid line) are in good agreement with the observed stages at B and C (filled circles) and that the model predictions exactly match the calibration stages at the upstream and downstream boundaries (open circles). It is further apparent from Fig. 6 that most of the stage attenuation occurs between A and B, where A is located at the tailwater pool. A similar validation procedure was performed at the C51 site for $Q = 0.28$ m^3/s, and the results are shown in S5 for $z_D = 1.707$ m, 1.737 m, 1.768 m, and 1.798 m, where all stages are relative to NAVD 88. These results also show that the hydrodynamic model calibrated by Manning's n accurately predicts the corresponding stages at B and

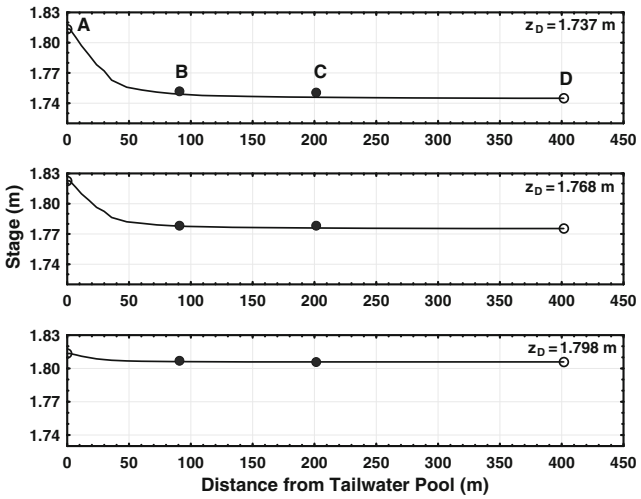

Fig. 6 Results of model validation at C43 site. Synoptic steady-state stages at A and D were used to calibrate the model, and synoptic steady-state stages at B and C were used to validate the model

C, and that most of the stage attenuation also occurs between stations A and B.

Stage attenuation in the study area downstream of the inflow location (i.e., tailwater pool) is relatively rapid due to the diverging flow condition. Since Manning's n also has a controlling influence on the rate of stage attenuation for a given flow, conditions in the wetland area encompassing 90% of the stage attenuation (as predicted by the numerical flow model) were used to characterize the relationship between Manning's n and flow depth. The extent of this "90% attenuation zone" varies with hydraulic condition, and is defined as the area in which the stage is reduced by 90% or less of the stage difference between the upstream and downstream stages in the study area. As an illustration, a typical hydraulic condition at the C43 site corresponds to $Q = 0.28$ m^3/s, $z_A = 1.823$ m, and $z_D = 1.775$ m, which requires that $n = 0.535$ and has the attenuation zone shown in Fig. 2a. Also, a typical hydraulic condition at the C51 site corresponds to $Q = 0.28$ m^3/s, $z_A = 1.829$ m, and $z_D = 1.749$ m, which requires that $n = 0.680$ and has the attenuation zone shown in Fig. 2c. It is apparent from Fig. 2a and c that the attenuation zones have approximate radial symmetry and cover relatively small areas compared with the extent of the study area, which collectively indicates that the attenuation zone is mostly insensitive to imposed (rectangular) boundaries constraining the flow in the study areas. Elevation views of the water-surface and bed-elevation profiles along a line extending from the center of the tailwater pool to the downstream boundary of the study areas are shown in S6 for the C43 and C51 sites. It is apparent from S6 that the bed elevations within the study areas tend to decrease with (southerly) distance from the tailwater pool, hence the average bed elevation within the attenuation zone is higher than the downstream bed elevations. The average depth of flow in the attenuation zone was determined by dividing the volume of aboveground water in the attenuation zone by the plan area of the attenuation zone.

Results

The Manning's n corresponding to each of the calibration hydraulic conditions shown in Fig. 4 and S4 was determined using the procedure described in the previous section, and these results are plotted versus the average depth of flow, h, in Fig. 7a and b for the C43 and C51 sites, respectively. As a first approximation, the relationship between Manning's n and flow depth was determined by assuming that the n value in the marsh is the same as the n value in the halo, and this relationship can be approximated by the solid lines in Fig. 7a and b. At the C43 site, the average flow depth, h, in the attenuation zone ranged from approximately 13 to 18 cm, with corresponding n values ranging from approximately 0.9 to 0.3. At the C51 site, the average flow depth within the attenuation zone ranged from approximately 13 to 22 cm, with corresponding n values of approximately 1.1 to 0.4. Both study sites show a fairly rapid and approximately linear decrease in n with increasing flow depth, h. The n versus h relationship in the hardwood-halo areas shown in Fig. 7a and b (solid lines) were determined by assuming a uniform n over the entire study area. This approximation was necessary because there was no information regarding the relative n value in the downstream marsh area, and previous studies in Everglades sawgrass marsh have indicated n values in the same range as those found for the hardwood halos. For example, Swain et al. (2004) reported n values in the range of 0.26 to 0.61 and

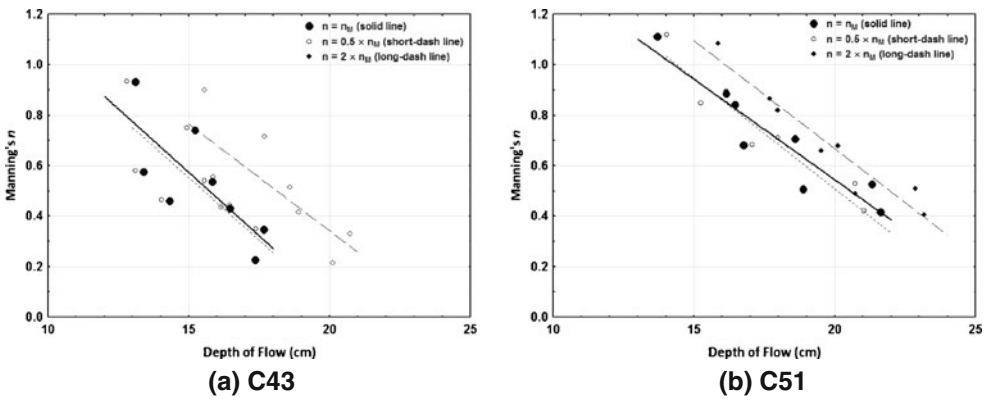

Fig. 7 Manning's n versus flow depth, h, at the study sites: **a** C43 site; and **b** C51 site. The solid lines approximate the n versus h relationship when the halo and marsh n values are equal, the short-dashed lines approximate the relationship when the halo n is one-half the marsh n, and the long-dashed lines approximate the relationship when the halo n is twice the marsh n

Variano et al. (2009) reported n values of 1.30 to 2.12 for sawgrass marsh, compared to n values of 0.23 to 1.11 for the hardwood halos as shown in Fig. 7a and b.

In spite of the plausible assumption of similarity in n values between hardwood halos and sawgrass marsh, in reality, the characteristic n values in the hardwood-dominated halos could be significantly different from the characteristic n values in the sawgrass-dominated marsh areas downstream of the halos. To determine what effect different n values in the downstream marsh area would have on the estimated n versus h relationship in the hardwood halo, sensitivity analyses were done and the results are reported below.

For all the results represented by the solid lines in Fig. 7a and b, the attenuation zone was entirely contained within the vegetation halo, and one would expect that as long as the attenuation zone is contained entirely within the halo the stage attenuation would be determined primarily by the Manning roughness in the halo and insensitive to the roughness assigned to the downstream marsh area. Under this circumstance, the n versus h relations shown by the solid lines in Fig. 7a and b would be representative of the hardwood-dominated halo. Field measurements at stations B and C as shown in Fig. 6 and S5 confirm that most of the stage attenuation occurs between A and B as predicted by the hydrodynamic model. The effect of the assumed marsh roughness on the n versus h relationship in the hardwood halo was investigated by repeating the determination of the n versus h relationship for cases in which the marsh roughness, n_M, is equal to twice the halo roughness, n, and also for the case where n_M is equal to one-half of n. These results are shown in Fig. 7a and b for the C43 and C51 sites, respectively. In both of the cases shown in Fig. 7, it is apparent that taking the marsh roughness to be equal to one-half the halo roughness yields almost the same relationship between n and h as is obtained by taking the marsh roughness as being equal to the halo roughness, thereby indicating that the derived n versus h relationship in the attenuation zone is insensitive to the assumed marsh roughness, provided that the marsh roughness is less than the halo roughness. In contrast, for the cases in which the marsh roughness is equal to twice the halo roughness, the n versus h relationship for the halo deviates from the n versus h relationship derived by assuming that the marsh roughness is equal to the halo roughness, thereby indicating that the estimated n versus h relationship in the halo is sensitive to the assumed marsh roughness. However, the linear relationship between n and h is apparent in all cases considered. The apparent reason for these results is that when the marsh roughness is less than the halo roughness the attenuation zone becomes smaller, and since the attenuation zone remains within the halo the n versus h relationship does not change. On the other hand, when the marsh roughness is greater than the halo roughness the attenuation zone becomes larger, extending beyond the halo, causing attenuation to be more affected by the assumed roughness in the downstream marsh area.

Discussion

It is shown in this study that, for the range of flow depths encountered, n values in the halo vegetation generally decrease (approximately) linearly with increasing flow depth. The n versus h relationship at the C43 and C51 sites are contrasted in Fig. 8a, where it is apparent that, for a given flow depth, n values at C51 are higher than at C43. This result suggests that, although the plant communities at these two halo locations are superficially similar, there are sufficient structural differences to lead to a significant difference in the n versus h relationship. Therefore, it is not possi-

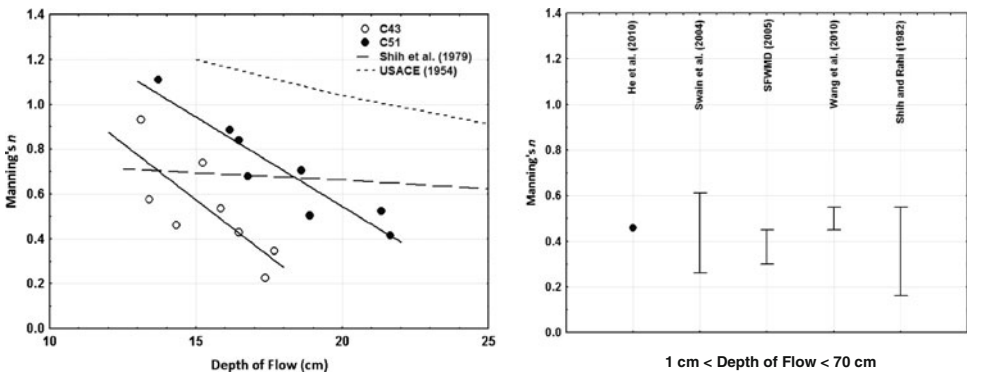

(a) Manning's n versus Depth **(b) Manning's n in Everglades Marsh**

Fig. 8 Manning's n versus flow depth, h, in the hardwood halos are shown in (**a**), and these results are compared with previous field measurements of n in Everglades sawgrass marsh shown in (**b**). Previous measurements of n versus h in Everglades marsh are also shown in (**a**)

ble to provide a general n versus h relationship for the vegetation halos.

Previous investigations of n versus h in South Florida marshes have been reported by Shih et al. (1979) and the U.S. Army Corps of Engineers (USACE 1954), and these results are contrasted with those determined in this study in Fig. 8a. Although Shih et al. (1979) and USACE (1954) are shown for comparative purposes in Fig. 8a, these previously reported results must be taken with some important caveats. Specifically, the Shih et al. (1979) data were collected in a marsh where water hyacinth, pickerel weed (*Pontederia lanceolata*), and buttonbush (*Cephalanthus occidentalis*) were the predominant vegetation species, in contrast to sawgrass, which is the predominant plant species downstream of the vegetation halo in the present study. Data showing the n values derived from more recent studies of south Florida marshes, like the marsh area found downstream of the vegetation halo, are shown in Fig. 8b. A value of n equal to 0.46 was found to best describe the results of He et al. (2010) and Swain et al. (2004) reported n values in the range of 0.26 to 0.61, values of n in the range of 0.30 to 0.45 were used for marshes in the South Florida Water Management Model (SFWMD 2005), and in modeling an area that included the current study areas Wang et al. (2007) found n values in the range of 0.45 to 0.55. Also shown in Fig. 8b is the range of n values reported by Shih and Rahi (1982), which were in the same marsh as reported in Shih et al. (1979). In contrast to these results, Variano et al. (2009) reported n values of 1.30 to 2.12 in a sawgrass-dominated area of the Florida Everglades and suggested that these higher-than-normal n values might be due to additional sources of drag at the scale of their experiments ($\sim$ 1 km) such as momentum dissipation in lateral shear layers. The flow depths in the aforementioned marsh studies were typically in the range of 1 to 70 cm for the numerical Everglades models of Swain et al. (2004), SFWMD (2005), and Wang et al. (2007), while the flow depths in Everglades field studies in sawgrass vegetation reported by He et al. (2010) and Variano et al. (2009) were in the ranges of 5 to 70 cm and 31 to 46 cm, and 40 to 65 cm, respectively. In the present study, the flow depths in the halo were in the range of 13 to 22 cm. Harvey et al. (2009) also investigated the flow resistance in Everglades sawgrass marsh but did not report their findings in terms of a Manning n, instead expressing their findings in terms of a vegetation drag coefficient. The field experiments reported in this paper had depth-based Reynolds numbers, Re_h, (in the hardwood halos) in the range of 2,800 to 8,700, which are comparable to the ranges of Reynolds numbers in the sawgrass experiments of Lee et al. (2004), $60 < \mathrm{Re}_h <$ 10,000; Harvey et al. (2009), $100 < \mathrm{Re}_h < 4{,}000$; and Variano et al. (2009), $630 < \mathrm{Re}_h < 920$.

Overall, the comparative results in Fig. 8b indicate that the n values in the marsh downstream of the halo area are likely to be in the range of 0.3 to 0.6, compared to the range of 0.2 to 1.1 found for the halos. The present study has found that in hardwood halos Manning's n decreases with increasing flow depth for depths in the range of 13 to 22 cm. A plausible explanation of this finding is that hardwood vegetation architecture and/or microtopography have a dominant effect at low flow depths. This is a consequence of the increased flow area with depth and the existence of more preferential flow pathways as the flow depth increases. A similar mechanism has been previously identified by Swain et al. (2004), who noted that when upscaling frictional resistance from point measurements at the field scale to represent an entire model grid, microtopography has the capability of increasing the effective frictional resistance at lower water depth. Areas with hardwood vegetation typically have much more open area than marshes, and tree trunks and fallen trees can create significant obstacles to flow, particularly at low flow depths.

Taken together, the results reported in this paper support the assertion that for low flow depths, less than 15–20 cm, the Manning n values are high in both the halo and downstream marsh vegetation. However, as the flow depths in both areas increase further, greater than 20 cm, the n values in the halo will likely become less than the n values in the marsh, which means that the hydraulic resistance that controls flow into the marsh will likely be the hydraulic resistance of the marsh rather than the hydraulic resistance of the halo. This result has particularly important water-management implications because it confirms that increased stages in the tailwater pool will generally lead to increased water deliveries, for the same stage difference between the tailwater pool and the marsh, and the halo vegetation will become less restrictive than the marsh vegetation in controlling water deliveries to Everglades National Park.

Acknowledgements This project was funded under Task Agreement J5297-09-0053 from the Everglades National Park. The U.S. Army Corps of Engineers, Jacksonville District, provided logistical support and funding of some support activities such as field topographic surveys. Patrick Kelly and Tommy Kiger at the University of Miami assisted in gathering the data, and Roy Sonenshein from Everglades National Park provided helpful insights while serving as the project manager. Alicia LoGalbo of Everglades National Park conducted field reconnaissance and identification of the plant communities, AMJ Environmental Inc. installed the field equipment and performed a field survey of reference elevations and ARC Surveying Inc.

performed a second field survey of the reference locations. The review comments of Laurel Larsen of USGS and an anonymous reviewer led to significant improvements in the original manuscript.

References

Chen C (1991) Unified theory on power laws for flow resistance. Journal of Hydraulic Engineering 117:371–389

Chin D (2006) Water-Resources Engineering, 2nd edn. Prentice-Hall, Upper Saddle River, New Jersey

Duever M, Meeder J, Meeder L, McCollum J (1994) The climate of south Florida and its role in shaping the Everglades ecosystem. In: Davis S, Ogden J (eds) Everglades: The ecosystem and its restoration. St. Lucie Press Delray Beach, Florida, pp 225–248

He G, Engel V, Leonard L, Croft A, Childers D, Laas M, Deng Y, Solo-Gabriele, H (2010) Factors Controlling Surface Water Flow in a Low-gradient Subtropical Wetland. Wetlands 30:275–286

Harvey J, Schaffranek R, Noe G, Larsen L, Nowacki D, O'Connor B (2009) Hydroecological factors governing surface water flow on a low-gradient floodplain. Water Resources Research 45:1–20

Ho D, Engel V, Variano E, Schmieder P, Condon M (2009) Tracer studies of sheet flow in the Florida Everglades. Geophysical Research Letters 36:1–6

Huang Y, Saiers J, Harvey J, Noe G, Mylon S (2008) Advection, dispersion, and filtration of fine particles within emergent vegetation of the Florida Everglades. Water Resources Research 44:1–13

Kadlec R (1990) Overland Flow in Wetlands: Vegetation Resistance. Journal of Hydraulic Engineering 116:691–705

Larsen L, Harvey J, Crimaldi J (2009) Predicting bed shear stress and its role in sediment dynamics and restoration potential of the Everglades and other vegetated flow systems. Ecological Engineering 35:1773–1785

Lee J, Roig L, Jenter H, Visser H (2004) Drag coefficients for modeling flow through emergent vegetation in the Florida Everglades. Ecological Engineering 22:237–248

Luhar M, Rominger J, Nepf H (2008) Interaction between flow, transport and vegetation spatial structure. Environmental Fluid Mechanics 8:423–439

Nepf H (1999) Drag, turbulence, and diffusion in the flow through emergent vegetation. Water Resources Research 35:479–489

Sauer VB (2002) Standards for the Analysis and Processing of Surface-Water Data and Information Using Electronic Methods. USGS Water-Resources Investigations Report 01–4044

Shih S, Federico A, Milleson J, Rosen M (1979) Sampling Programs for Evaluating Upland Marsh to Improve Water Quality. Transactions of the American Society of Civil Engineers 22:828–833

Shih S, Rahi G (1982) Seasonal Variations of Manning's Roughness Coefficient in a Subtropical Marsh. Transactions of the American Society of Civil Engineers 25:116–119

South Florida Water Management District (2005) Documentation of the South Florida Water Management Model, Version 5.5. West Palm Beach, Florida

Swain E, Wolfert M, Bales J, Goodwin C (2004) Two-dimensional hydrodynamic simulation of surface-water flow and transport to Florida Bay through the Southern Inland and Coastal Systems (SICS). Water-Resources Investigations Report No. 03-4287, United States Geological Survey

Tsihrintzis V (2001) Discussion of Wu et al., 1999. Journal of Hydraulic Engineering 127:241–244

Tsihrintzis V, Madiedo E (2000) hydraulic resistance determination in marsh wetlands. Water Resources Management 14:285–309

U.S. Army Corps of Engineers (1954) Central and Southern Florida Project: Part IV, Section 7, Design Memorandum, Interim Report on Evaluation of Manning's n Vegetated Areas, Serial Number 32, Jacksonville, Florida, U.S. Army Corps of Engineers Regional Office

U.S. Army Corps of Engineers (2008) Users Guide To RMA2WES Version 4.5. U.S. Army, Engineer Research and Development Center Waterways Experiment Station Coastal and Hydraulics Laboratory

Variano E, Ho D, Engel V, Schmieder P, Reid M (2009) Flow and mixing dynamics in a patterned wetland: Kilometer-scale tracer releases in the Everglades. Water Resources Research 45:1–11

Wang J, Swain E, Wolfert M, Langevin C, James D, Telis P (2007) Application of FTLOADDS to Simulate Flow, Salinity, and Surface-Water Stage in the Southern Everglades, Florida. Scientific Investigations Report No. 2007-5010, United States Geological Survey